

XSleepNet: Multi-View Sequential Model for Automatic Sleep Staging

Huy Phan, Oliver Y. Chén, Philipp Koch, Alfred Mertins, and Maarten De Vos

Abstract—Automating sleep staging is vital to scale up sleep assessment and diagnosis to millions of people experiencing sleep deprivation and disorders and to enable longitudinal sleep monitoring in home environments. Learning from raw polysomnography signals and their derived time-frequency image representations has been prevalent. However, learning from multi-view inputs (e.g. both the raw signals and the time-frequency images) for sleep staging is difficult and not well understood. This work proposes a sequence-to-sequence sleep staging model, XSleepNet, that is capable of learning a joint representation from both raw signals and time-frequency images effectively. Since different views often generalize (and overfit) at different rates, the proposed network is trained in such a way that the learning pace on each view is adapted based on their generalization/overfitting behavior. In simple terms, the learning on a particular view is speeded up when it is generalizing well and slowed down when it is overfitting. View-specific generalization/overfitting measures are computed on-the-fly during the training course and used to derive weights to blend the gradients from different views. As a result, the network is able to retain representation power of different views in the joint features which represent the underlying distribution better than those learned by each individual view alone. Furthermore, the XSleepNet architecture is principally designed to gain robustness to the amount of training data and to increase the complementarity between the input views. Experimental results on five databases of different size show that XSleepNet consistently results in better performance than the single-view baselines as well as the multi-view baseline with a simple fusion strategy. Finally, XSleepNet outperforms all prior sleep staging methods and sets new state-of-the-art results on the experimental databases.

Index Terms—Automatic sleep staging, deep neural network, multi-view learning, gradient blending, sequence-to-sequence, end-to-end.

1 INTRODUCTION

Anyone who has experienced a sleepless night would acknowledge the importance of sleep in maintaining our mental and physical health [1], [2]. Unfortunately, a lack of sleep and sleep disorders are prevalent and affecting millions of people worldwide, imposing serious public health crisis [3]. For example, 50 to 70 millions of Americans suffer from a chronic sleep or wakefulness disorder, such as insomnia, narcolepsy, restless legs syndrome, and sleep apnea [4]. Additionally, medical errors due to sleep deprivation has caused 100 thousands death in US hospitals. Consequently, there is an increasing demand for accurate sleep assessment and diagnosis and the technological quest for longitudinal sleep monitoring in home environments [5], [6]. In order to address these challenges, sleep scoring [7], [8], an indispensable step in sleep assessment and diagnosis, needs to be automated since labor-intensive and time-consuming manual scoring becomes difficult to handle large-scale sleep data. To see this, consider a task to score an overnight polysomnography (PSG) recording: it takes a sleep expert about two hours to complete the task manually [9]; in contrast, a machine can complete the same task in a few seconds.

- *H. Phan is with the School of Electronic Engineering, Queen Mary University of London, London, UK, E1 4NS. E-mail: h.phan@qmul.ac.uk*
- *O. Y. Chén is with the Department of Engineering Science, University of Oxford, Oxford, UK, OX1 3PJ.*
- *P. Koch and A. Mertins are with the Institute for Signal Processing, University of Lübeck, Lübeck, Germany, 23562.*
- *M. De Vos is with the Department of Electrical Engineering (ESAT), KU Leuven, Leuven, Belgium, 3001.*

The sleep research community is witnessing a unprecedented progress in automatic sleep staging on which machine's performance is approaching to sleep experts' [10], [11]. The closing gap is enabled, in part, by the ever-growing annotated sleep databases. Using large-scale data, novel sleep scoring methods can be developed and tested under powerful deep learning paradigms [11], [12], [13], [14], [15]. Since the very first few attempts [16], [17], deep learning for automatic sleep staging has evolved rapidly in both designing targeted modelling methodologies and building effective network architectures. The standard one-to-one [18], [19] and many-to-one [17], [20] are beginning to be replaced with one-to-many (i.e. multitasking) [21] and many-to-many (i.e. sequence-to-sequence) frameworks [10], [22] that better represent the sequential nature of sleep data. Concerning network architectures, the vanilla ones, such as Deep Belief Networks (DBNs) [16], Auto-encoders [23], Deep Neural Networks (DNNs) [24], Convolutional Neural Networks (CNNs) [17], [18], [20], [21], [25], [26], and Recurrent Neural Networks (RNNs) [19] are being surpassed by more complex, task-specific architectures such as DNN+RNN [24], CNN+RNN [22], and hierarchical RNN [10].

Existing work on automatic sleep staging can be categorized based on the types of signal input of the network. There are two main categories: the first directly processes 1-dimensional raw signals [17], [20], [22], [24], [26], [27], [28] and the second ingests 2-dimensional time-frequency images as inputs [10], [11], [18], [19]. A time-frequency image is usually derived from a raw signal via some transformations, for example short-time Fourier transform (STFT), and is,

in general, considered as a higher-level representation of the raw signal. However, one cannot conclude that one is better than the other as the performance of an automatic sleep staging system depends on many other factors, such as the amount of training data, the network architecture, etc. Rather, they should be considered as two different views regarding the same underlying data distribution; when used together, they should complement each other and improve performance of the task at hand when used jointly. Indeed, prior work [13], [14], [15] has attempted to combine both raw signals and time-frequency images in the same network to tackle automatic sleep staging. Such a network is designed to have a subnet dedicated to an input type. The learned features from different network subnets are then combined (for example, via concatenation) to form joint features on which classification are made.

In general, learning representations that capture information from multiple views should benefit recognition models [29], [30]. Confusingly, combining multiple input types in a deep network often results in a performance drop rather than an improvement, as we will show in our experiments. This observation has not been well understood. In this work, we will demonstrate that a simple strategy like concatenation (as in [13], [14], [15]) for learning from multi-view input is suboptimal. We will also illustrate why a multi-view network often results in worse performance than the best single-view counterpart. To address this issue, we propose a sequence-to-sequence network, XSleepNet, that can learn joint features from both raw and time-frequency input effectively. During training, the network is able to oversee overfitting/generalization behavior on each input view and uses this information to adapt its contribution into the joint-feature learning via gradient blending. Simply put, learning on the view that is generalizing well will be encouraged while the view that is overfitting will be impeded from learning. In addition, we layout the principles that guides the XSleepNet architecture to achieve robustness (to amount training data) and complementarity (i.e. how the two input views complement one another). To evaluate the efficacy of the model, we conducted experiments on five databases with different sizes and show that the proposed XSleepNet outperforms both three strong baselines as well as other methods applied to these databases in prior work. Importantly, unlike the typical fusion strategy, XSleepNet is able to consolidate the representation power of the input views to produce the joint features which better represent the underlying data distribution, and therefore, result in higher performance than single views.

The rest of the article is organized as follows. We outline the principles guiding the network design in Section 2. We then describe the network architecture and its multi-view joint learning mechanism in Section 3. Details about the experiments will be presented in Section 4, followed by discussion in Section 5. We conclude the article in Section 6.

2 DESIGN PRINCIPLES

As a multi-view model, XSleepNet is composed of two network streams: one for the raw signal and the other one for the time-frequency image. The following design principles aim to introduce robustness (to amount of training data)

and complementarity (i.e. how the two input views complement one another) into the network while maintaining its flexibility to learn from multiple views effectively.

Principle 1 (Robustness): The raw-data network stream is large while the time-frequency one is compact in terms of model size. Specifically, the former has 5.6×10^6 parameters in total, about 35 times larger than 1.6×10^5 parameters of the latter. In general, the footprint of a deep network is proportional to its modelling capacity and should be devised depending on the amount of training data available. The rule of thumb is to increase the network capacity when the training data is large and vice versa. However, this is not trivial, especially for clinicians, who may not be technology-aware. With two network streams with varying modelling capacity, XSleepNet is robust in terms of performance regardless the amount of training data. When the training data is small, the higher-capacity stream may overfit, but the lower-capacity one generalizes well. When the training data is large, the lower-capacity may underfit, but the higher-capacity stream generalizes well. Combining the two streams results in a balanced, and generalizable model. This is possible owing to the generalization- and overfitting-aware training procedure of the network (*Principle 3*).

Principle 2 (Complementarity): The two network streams have diverging architectures. Theoretically, for a joint model to be effective, each individual model should be diversified [31]. Practically, there is empirical evidence suggesting that CNNs with raw signals and RNNs with time-frequency images are complementary on their sleep staging outputs. For example, the former is favorable for N3, and the latter works better for N1 and REM on MASS database [10], [32]. We therefore design XSleepNet such that the raw stream is based on a CNN architecture and the time-frequency stream is based on an RNN architecture to extract epoch-wise features. Even when an RNN is required for inter-epoch sequential modelling, different types of RNN cells are used in the two network streams (see more details in the next section) to secure the diversification.

Principle 3 (Generalization- and overfitting-aware training): The multi-view network is trained in such a way that learning on the network stream that is generalizing well is accelerated while the overfitting one is impeded. This principle is a requirement without which the multi-view network would fail to produce better representation than both the single-view network streams when they are trained separately. In literature, a network with multiple input types typically combines the features learned from the constituent streams (e.g., via concatenation [13], [14], [15]) to form the joint representation which then serves the classification purpose. This is illustrated in Fig. 1 (a). As a result, there is no viable way to regulate the learning pace of the streams individually. This would not be a problem if the network streams generalize and overfit at the same time. However, this is not often the case, as illustrated via their validation losses in Fig. 1 (b). In turn, the validation loss of the simple combination appears to be averaged out as illustrated in the figure, suggesting worse generalization than the best single-view network stream.

In order to regulate the learning pace of the network streams, it is necessary to gain access to their gradient flows. In XSleepNet, in addition to the joint classification

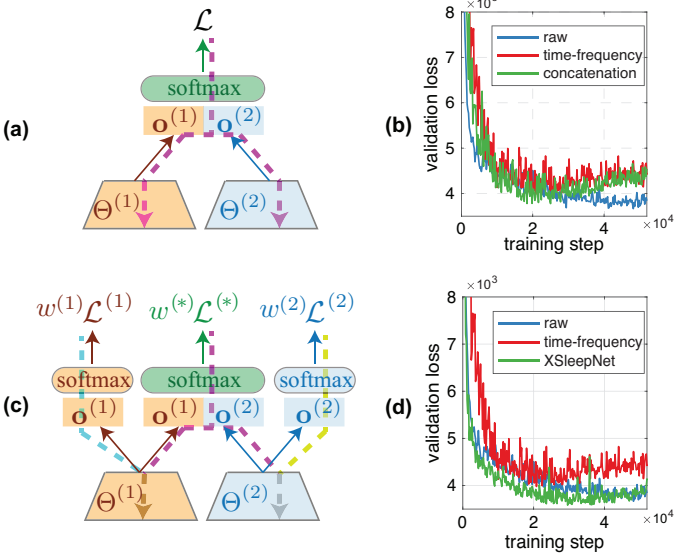


Fig. 1: Illustration of multi-view learning with simple concatenation and the proposed XSleepNet. Joint multi-view learning with simple concatenation (a) and its resulting validation loss in comparison that of single-view training (b). Joint multi-view learning with XSleepNet (c) and its resulting validation loss in comparison that of single-view training. In (a) and (c), the dash lines represent the gradient flows. Θ , \mathbf{o} , and \mathcal{L} denote a network stream corresponding to one input view, a learned feature vector, and a loss value, respectively. The superscripts, i.e. (1) and (2), indicate the input view specifically. In addition, in (c), w denotes a weight and the superscript (*) indicates the joint network branch.

branch, two additional branches are added. Different from the joint classification branch, these two newly introduced branches operate on the stream-wise features as illustrated in Fig. 1 (c). By monitoring the generalization/overfitting behavior (see more details in Section 3.2) of the classification branches, we are able to weight their gradient flows so that the one that generalizes well is awarded with a large weight and the one that overfits is given a small weight. By doing so, we blend the gradients according to the generalization and overfitting behavior of the classification branches and individualize the learning pace of the network streams. Unlike the simple concatenation (see Fig. 1 (b)), with this adaptive gradient blending approach, XSleepNet results in a better joint representation of the underlying data distribution than that of the single-view networks, as evidenced by its validation loss in Fig. 1 (d).

3 XsleepNet

3.1 Architecture

Given a training set $\{\mathcal{S}_n\}_{n=1}^N$ of size N where $\mathcal{S} = \left(\left\{(\mathbf{S}_1^{(1)}, \mathbf{S}_1^{(2)}), \mathbf{y}_1\right\}, \dots, \left\{(\mathbf{S}_L^{(1)}, \mathbf{S}_L^{(2)}), \mathbf{y}_L\right\}\right)$ is a sequence of L sleep epochs. $\mathbf{S}_l^{(1)}$ and $\mathbf{S}_l^{(2)}$ represent two different views (i.e. inputs of two different types) and $\mathbf{y}_l \in \{0, 1\}^Y$ denotes the one-hot encoding label of the l -th epoch, $1 \leq l \leq L$. In this context, $\mathbf{S}_l^{(1)} \in \mathbb{R}^{3000 \times C}$

is a C -channel 30-second raw signal sampled at 100 Hz and $\mathbf{S}_l^{(2)} \in \mathbb{R}^{F \times T \times C}$ is the time-frequency representation, with $F = 129$ frequency bins and $T = 29$ time points (see more details in Section 4). Here, C takes a value of $\{1, 2, 3\}$ depending on the used channel combination (i.e. EEG, EEG-EOG, or EEG-EOG-EMG). In addition, $Y = 5$ since we consider classification of 5 sleep stages in this work.

The proposed XSleepNet architecture is illustrated in Fig. 2 where the network stream in orange handles the raw signal and the one in blue deals with the time-frequency image. Long-term (i.e. inter-epoch) sequential modelling is the heart of sequence-to-sequence sleep staging models, including XSleepNet. In light of this, we employ bidirectional RNNs for this purpose as in [10], [22]. The raw and time-frequency inputs are therefore encoded into two sequences of output vectors:

$$(\mathbf{o}_1^{(1)}, \dots, \mathbf{o}_L^{(1)}) = GRU(\mathcal{F}_1(\mathbf{S}_1^{(1)}), \dots, \mathcal{F}_1(\mathbf{S}_L^{(1)})), \quad (1)$$

$$(\mathbf{o}_1^{(2)}, \dots, \mathbf{o}_L^{(2)}) = LSTM(\mathcal{F}_2(\mathbf{S}_1^{(2)}), \dots, \mathcal{F}_2(\mathbf{S}_L^{(2)})), \quad (2)$$

respectively. With respect to the design principle 2, the bidirectional RNN in (1) is realized by Gated Recurrent Unit (GRU) cells [33] and the one in (2) is realized by Long Short-Term Memory (LSTM) cells [34] coupled with recurrent batch normalization [35]. In (1) and (2), $\mathbf{o}_l^{(1)} \in \mathbb{R}^{2H_1}$ and $\mathbf{o}_l^{(2)} \in \mathbb{R}^{2H_2}$, $1 \leq l \leq L$, where H_1 and H_2 are the sizes of the GRU and LSTM cells' hidden state vectors, respectively. \mathcal{F}_1 and \mathcal{F}_2 denote the subnetworks that play the role of a feature map to transform an input epoch into a feature vector of high-level representation. They are separately tailored for raw and time-frequency inputs with respect to design principle 2.

Feature map \mathcal{F}_1 : In order to transform a raw signal $\mathbf{S}^{(1)}$ into a high-level feature $\mathbf{x}^{(1)}$, the feature map $\mathcal{F}_1 : \mathbf{S}^{(1)} \mapsto \mathbf{x}^{(1)}$ is realized by a *fully* convolutional neural network (FCNN) [36]. Without confusion, the subscript l is omitted here for simplicity. The network consists of 9 strided one-dimensional convolutional layers [36] with a common filter width of 31 and stride length of 2. The convolutional layers are designed to have their numbers of filter increased along the network's depth, taking values of 16, 16, 32, 32, 64, 64, 128, 128, and 256, to compensate for the gradually smaller induced feature maps. Given the input $\mathbf{S}^{(1)}$ of size $3000 \times C$, the CNN results in feature map sizes of 1500×16 , 750×16 , 325×32 , 163×32 , 82×64 , 41×64 , 21×128 , 11×128 , and 6×256 after the 9 convolutional layers, respectively. In addition, each convolutional layer is followed by parametric rectified linear units (PReLU) [37]. The output of the last convolutional layer is flattened to form the induced epoch-wise feature vector $\mathbf{x}^{(1)} = \mathcal{F}_1(\mathbf{S}^{(1)}) \in \mathbb{R}^{1536}$.

Feature map \mathcal{F}_2 : Different from \mathcal{F}_1 , the feature map $\mathcal{F}_2 : \mathbf{S}^{(2)} \mapsto \mathbf{x}^{(2)}$ relies on attention-based RNN coupled with learnable *filterbank layers* to map a time-frequency input $\mathbf{S}^{(2)}$ to a high-level feature vector $\mathbf{x}^{(2)}$. Again, the subscript l is omitted for simplicity. First, each channel of $\mathbf{S}^{(2)}$ is preprocessed by a learnable filterbank layer of D filters as in [10], [18] so that its spectral dimension is smoothed and reduced from F to D frequency bins, resulting in $\mathbf{S}'^{(2)} \in \mathbb{R}^{T \times D \times C}$. Afterwards, $\mathbf{S}'^{(2)}$ is interpreted as a sequence of T vectors

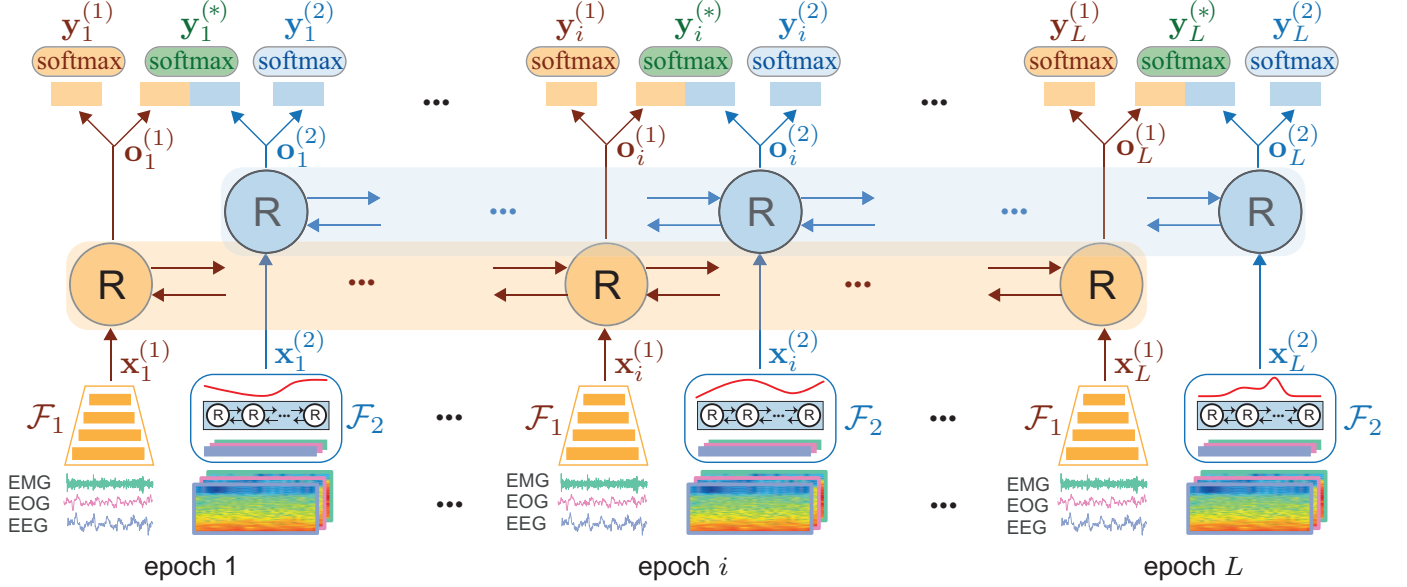


Fig. 2: Illustration of the proposed XSleepNet architecture. The network streams in orange and blue corresponds to the raw and time-frequency image inputs, respectively.

$(\mathbf{s}'_1, \dots, \mathbf{s}'_T)$, where each $\mathbf{s}'_t \in \mathbb{R}^{DC}, 1 \leq t \leq T$, and encoded by a bidirectional RNN into a sequence of vectors $(\mathbf{z}_1, \dots, \mathbf{z}_T)$:

$$(\mathbf{z}_1, \dots, \mathbf{z}_T) = LSTM(\mathbf{s}'_1, \dots, \mathbf{s}'_T). \quad (3)$$

Here the bidirectional RNN is realized by LSTM cells [34] coupled with recurrent batch normalization [35] and $\mathbf{z}_t \in \mathbb{R}^{2H}$ with H equal to the size of the LSTM cells' hidden state vectors. Note that this bidirectional RNN here is for short-term (i.e. intra-epoch) sequential modelling and should not be confused with the one for inter-epoch sequential modelling in (2). The induced epoch-wise feature vector $\mathbf{x}^{(2)}$ is eventually obtained via a weighted combination of the vectors $\mathbf{z}_1, \dots, \mathbf{z}_T$:

$$\mathbf{x}^{(2)} = \sum_{t=1}^T \alpha_t \mathbf{z}_t, \quad (4)$$

where $\alpha_1, \dots, \alpha_T$ are attention weights learned by an attention layer as in [10], [19].

In light of the design Principle 2, it is worth noting that the way \mathcal{F}_1 and \mathcal{F}_2 learn to produce features are distinguishable. We conjecture that, due to its reliance on FCNN, \mathcal{F}_1 can capture temporal-equivariant patterns from the raw input. That is, such a feature can occur at any time point in the 30-second duration of the raw signal. For example, micro events such as K-complex and sleep spindle [7], [8] frequently appearing in the sleep stage N2 have this characteristic. On the other hand, built upon the bidirectional RNN and the attention mechanism, \mathcal{F}_2 can encode the sequential patterns of the spectral columns in its time-frequency image input. This is useful to capture features with a sequential structure such as the theta wave activity in the sleep stage N1 [7], [8].

Adhering to the design Principle 3, the proposed XSleepNet accommodates three softmax branches for classification: the first two are view-specific (i.e. operating on the output vectors of the raw and time-frequency network streams specifically) and the third one for the joint view

(i.e. operating on the joint feature vector), as illustrated in Fig. 1. Given the output sequence $(\mathbf{o}_1^{(1)}, \dots, \mathbf{o}_L^{(1)})$ in (1) and $(\mathbf{o}_1^{(2)}, \dots, \mathbf{o}_L^{(2)})$ in (2), we obtain three sequences of classification labels $(\hat{\mathbf{y}}_1^{(1)}, \dots, \hat{\mathbf{y}}_L^{(1)}), (\hat{\mathbf{y}}_1^{(2)}, \dots, \hat{\mathbf{y}}_L^{(2)}),$ and $(\hat{\mathbf{y}}_1^{(*)}, \dots, \hat{\mathbf{y}}_L^{(*)})$ via the three classification layers, where

$$\hat{\mathbf{y}}_l^{(1)} = softmax^{(1)}(\mathbf{o}_l^{(1)}), \quad (5)$$

$$\hat{\mathbf{y}}_l^{(2)} = softmax^{(2)}(\mathbf{o}_l^{(2)}), \quad (6)$$

$$\hat{\mathbf{y}}_l^{(*)} = softmax^{(*)}([\mathbf{o}_l^{(1)} \oplus \mathbf{o}_l^{(2)}]), 1 \leq l \leq L, \quad (7)$$

and \oplus denotes vector concatenation.

During training, the losses induced by these three classification branches are used to compute the weights for gradient blending (cf. Section 3.2). When the trained network is evaluated on the test data, either the joint output $(\hat{\mathbf{y}}_1^{(*)}, \dots, \hat{\mathbf{y}}_L^{(*)})$ or a weighted ensemble of the three outputs can be considered as final outputs (cf. Section 3.3).

3.2 Adaptive Gradient Blending for Multi-View Joint Training

Given three classification outputs $(\hat{\mathbf{y}}_1^{(1)}, \dots, \hat{\mathbf{y}}_L^{(1)}), (\hat{\mathbf{y}}_1^{(2)}, \dots, \hat{\mathbf{y}}_L^{(2)}),$ and $(\hat{\mathbf{y}}_1^{(*)}, \dots, \hat{\mathbf{y}}_L^{(*)})$, the cross-entropy losses induced by the three classification branches are

$$\mathcal{L}^{(k)} = -\frac{1}{L} \sum_{l=1}^L \mathbf{y}_l \log(\hat{\mathbf{y}}_l^{(k)}), \quad (8)$$

where $k \in \{1, 2, *\}$. In order to balance the generalization/overfitting rate of the classification branches, we weight the losses adaptively to schedule the learning on the two network streams. Similar to [38], we computed the loss weights using the ratio of generalization and overfitting measures:

$$w^{(k)} = \frac{1}{Z} \frac{G_k}{O_k^2}, \quad (9)$$

In (9), Z is a normalization factor. The generalization measure G_k is defined as the gained information about the target distribution we learn from training. On the other hand, the overfitting measure O_k is defined as the gap between the gain on the training set and the target distribution. Here, G_k and O_k are approximated as:

$$G_k \approx \mathcal{L}_{\diamond}^{(k)}(0) - \mathcal{L}_{\diamond}^{(k)}(n), \quad (10)$$

$$O_k \approx \left(\mathcal{L}_{\text{train}}^{(k)}(0) - \mathcal{L}_{\diamond}^{(k)}(0) \right) - \left(\mathcal{L}_{\text{train}}^{(k)}(n) - \mathcal{L}_{\diamond}^{(k)}(n) \right), \quad (11)$$

where $\mathcal{L}_{\text{train}}^{(k)}(n)$ and $\mathcal{L}_{\diamond}^{(k)}(n)$ denote the training loss and the true loss at the training step n , respectively. In practice, $\mathcal{L}_{\diamond}^{(k)}(n)$ is unknown and we approximate it by the loss evaluated on a held-out validation set, $\mathcal{L}_{\text{valid}}^{(k)}(n)$. To reduce the computational cost of obtaining $\mathcal{L}_{\text{train}}^{(k)}(n)$ on the entire training set, only a subset randomly sampled from the training set is used for this purpose.

The weighted loss used for network training at the training step n is then given by:

$$\mathcal{L}(n) = \sum_{k \in \{1, 2, *\}} w_{\diamond}^{(k)}(n) \mathcal{L}^{(k)}(n). \quad (12)$$

3.3 Self-ensemble

Besides the joint-view output $(\hat{y}_1^{(*)}, \dots, \hat{y}_L^{(*)})$ which can be considered as the final outputs of the network, one can leverage the availability of the network's three outputs to form a self-enssembled decisions. When applying the trained model on a test recording, one may advance the input sequence of length L by one epoch at a time as in [10], [32], and as a result, L decisions are obtained for every epoch from each classification branch. The log likelihood of a sleep stage $c \in \{W, N1, N2, N3, REM\}$ at the i -th epoch after self-ensembling is therefore

$$\log P(y_i = c) = \sum_{k \in \{1, 2, *\}} \sum_{j=i-L+1}^i \log \left(w_{\diamond}^{(k)} P^{(k)}(y_i = c | \mathcal{S}_j) \right). \quad (13)$$

In the above equation, $P^{(k)}(y_i = c | \mathcal{S}_j)$ denotes the probability that the classification branch k predicts the sleep stage c at the i -th epoch given the input sequence \mathcal{S}_j starting from the j -th epoch. We use $w_{\diamond}^{(k)}$ to denote the loss weight of the classification branch k found with the final model. The output sleep stage \hat{y}_i at the i -th epoch is determined via log likelihood maximization:

$$\hat{y}_i = \underset{c}{\operatorname{argmax}} \log P(y_i = c), \quad (14)$$

where $c \in \{W, N1, N2, N3, REM\}$.

4 EXPERIMENTS

4.1 Databases

We employed five publicly available databases in this study: SleepEDF-20, SleepEDF-78, Montreal Archive of Sleep Studies (MASS), Physionet2018, and Sleep Heart Health Study (SHHS). A summary of the adopted databases is shown in Table 1.

SleepEDF-20: This is the Sleep Cassette (SC) subset of the Sleep-EDF Expanded dataset [39], [40] (version 2013),

consisting of 20 subjects (10 males and 10 females) aged 25-34. Two consecutive day-night PSG recordings were collected for each subject, except for subject 13 who has one night's data lost due to device failure. Each 30-second PSG epoch was manually labelled into one of eight categories {W, N1, N2, N3, N4, REM, MOVEMENT, UNKNOWN} by sleep experts according to the R&K standard [8]. Similar to previous works [17], [18], [19], [21], [22], [23], N3 and N4 stages were considered as N3 collectively and MOVEMENT and UNKNOWN categories were excluded. We adopted the Fpz-Cz EEG and ROC-LOC EOG (i.e. the EOG horizontal) channels in this study. However, we did not experiment with EMG as full EMG recordings are not available.

SleepEDF-78: This database is the 2018 version of Sleep-EDF Expanded dataset [39], [40], consists of 78 healthy Caucasian subjects aged 25-101. Similar to SleepEDF-20, two consecutive day-night PSG recordings were collected for each subject, except subjects 13, 36, and 52 whose one recording was lost due to device failure. Manual scoring was done by sleep experts according to R&K standard [8] and each 30-second PSG epoch was labeled as one of eight categories W, N1, N2, N3, N4, REM, MOVEMENT, UNKNOWN. N3 and N4 stages were merged into N3 stage. MOVEMENT and UNKNOWN epochs were excluded. We used the Fpz-Cz EEG and ROC-LOC EOG in this study and no experiments were carried out with EMG due to its unavailability.

MASS: This database was pooled from different hospital-based sleep laboratories, consisting of whole-night recordings from 200 subjects (97 males and 103 females) aged 18-76. Manual annotation was accomplished by sleep experts according to the AASM standard [7] (SS1 and SS3 subsets) or the R&K standard [8] (SS2, SS4, and SS5 subsets). As in [10], [21], we converted R&K annotations into five sleep stages {W, N1, N2, N3, and REM} as of the AASM standard. Epochs with a length of 20 seconds were expanded to 30-second ones by including 5-second segments before and after them. We used the C4-A1 EEG, ROC-LOC EOG, and CHIN1-CHIN2 EMG in our experiments.

Physio2018: This database contributed by Massachusetts General Hospitals Computational Clinical Neurophysiology Laboratory and used in the 2018 Physionet challenge [40], [41], which aimed to detect arousal during sleep from PSG data. We employed the training set (annotation of the evaluation set was not publicly available) consisting of 944 subjects aged 18-90 in the experiments. Manual scoring was done by sleep experts according to the AASM guideline [7]. C3-A2 EEG, E1-M2 EOG, and CHIN1-CHIN2 EMG were used.

SHHS: The SHHS database [42], [43] was collected from multiple centers to study the effect of sleep-disordered breathing on cardiovascular diseases. It has two rounds of PSG records, namely Visit 1 (SHHS-1) and Visit 2 (SHHS-2). The former consisting of 5,791 subjects aged 39-90 was employed in this work. Manual scoring was completed using the R&K guideline [8]. Similar to other databases annotated with the R&K rule, N3 and N4 stages were merged as N3 stage and MOVEMENT and UNKNOWN epochs were discarded. We adopted C4-A1 EEG, ROC-LOC EOG, and bipolar submental EMG in the experiments.

These databases were adopted in this work to showcase

TABLE 1: Summary of the employed databases.

Database	Size	EEG channel	EOG channel	EMG channel	Scoring method	Experimental setup	Held-out validation set	Random training subset
SleepEDF-20	20	Fpz-Cz	ROC-LOC	—	R&K	20-fold CV	4 subjects	4 subjects
SleepEDF-78	79	Fpz-Cz	ROC-LOC	—	R&K	10-fold CV	7 subjects	7 subjects
MASS	200	C4-A1/C3-A2	ROC-LOC	CHIN1-CHIN2	AASM/R&K	20-fold CV	10 subjects	10 subjects
Physio2018	994	C3-A2	E1-M2	CHIN1-CHIN2	AASM	5-fold CV	50 subjects	50 subjects
SHHS	5,791	C4-A1	ROC-LOC	Submental EMG	R&K	train/test: 0.7/0.3	100 subjects	100 subjects

the robustness of the proposed XSleepNet in dealing with datasets of different sizes, which is one of the guiding principles of the network design (see more details in Section 2). For each database, we experimented with single-channel EEG, 2-channel EEG·EOG, and 3-channel EEG·EOG·EMG combinations as inputs when possible. Particularly, only single-channel and 2-channel experiments were conducted on SleepEDF-20 and SleepEDF-78 since they do not have a full EMG channel available in the PSG recordings. All the signals were resampled to 100 Hz.

We conducted experiments following the data splits as summarized in Table 1. These data splits have been commonly used in literature, enabling a direct performance comparison between our system and prior work. As noted in the table, a number of subjects were held out for validation. Particularly, for the SHHS database, although we followed Sors *et al.* [26] to randomly sample and leave out 30% of subjects as the test set, we did not leave out a validation set as large as 20% of the subjects but 100 as we empirically found 100 subjects were sufficient for validation purpose. Furthermore, a random subset was also drawn from the training subjects for computing the loss weights as described in Section 3.2. Of note, different from the validation set, which is not involved in network training, this training subset contributes to the training process as usual. The performance was then computed over all the cross-validation folds.

4.2 Parameters

To extract the time-frequency input mentioned in Section 4.2, a signal (i.e., EEG or EOG or EMG) of a 30-second PSG epoch sampled at 100 Hz was divided into two-second windows with 50% overlap, multiplied with a Hamming window, and transformed to the frequency domain by means of a 256-point Fast Fourier Transform (FFT). The amplitude spectrum was then log-transformed. The time-frequency images extracted from a database were normalized to zero mean and unit standard deviation before network training and testing.

The network implementation was based on *Tensorflow* framework [44]. The input sequence length was set to $L = 20$ which was proven to be a reasonable value for sequence-to-sequence models [10]. The feature map \mathcal{F}_2 was designed with $D = 32$ filters in each filterbank layer and 64 units in its LSTM cells’ hidden state vectors. The LSTM and GRU cells responsible for inter-epoch sequential modelling have 256 and 64 units in their hidden state vectors, respectively. Throughout the network, dropout [45] was applied during training with a dropout rate of 0.5 and 0.25 used for

convolutional layers and recurrent layers of the network, respectively.

The network was trained for 10 epochs using Adam optimizer [46] with a learning rate of 10^{-4} and a minibatch size of 32. The model was validated on the validation set every 200 training steps and the loss weights were also updated at the same time according to (9). The training process was stopped after 200 validation times if no accuracy improvement was recorded on the validation set.

4.3 Baselines

To assess the efficacy of the proposed XSleepNet, in addition to relevant prior work, we developed three baseline systems for performance comparison. (1) The first two baselines, *FCNN+RNN* and *ARNN+RNN*, are equivalent to the raw and time-frequency network streams shown in Fig. 2, respectively, but they were trained separately. Note that the *ARNN+RNN* is similar to SeqSleepNet presented in [10]. The third baseline, denoted as *Naive Fusion*, combines the multi-view features in a concatenate fashion (i.e. without adaptive gradient blending) and shares a similar network architecture to that of the proposed XSleepNet.

The networks were evaluated using five overall metrics, including accuracy, macro F1-score (MF1) [47], Cohen’s kappa [48], average sensitivity, and average specificity.

4.4 Experimental results

To give an overview of the performance of XSleepNet and the baselines, we collate and contrast their overall performance across all the experimental databases and channel combinations in Fig. 3. Here, XSleepNet-SE represents the XSleepNet with self-ensemble described in Section 3.3.

Fig. 3 reveals several compelling patterns. First, between the two single-view baselines, *ARNN+RNN* and *FCNN+RNN*, the former often results in better performance when the data size is relatively small, for example in SleepEDF-20, SleepEDF-78 (EEG·EOG), and MASS. The opposite is commonly seen with larger databases, such as in Physio2018 and SHHS (EEG). These patterns can be partly explained by the difference in their model footprints: the *ARNN+RNN* with single-channel EEG input has about 1.6×10^5 parameters in total, 35 times smaller than 5.6×10^6 parameters of the *FCNN+RNN* counterpart. As a result, *FCNN+RNN* is prone to overfitting on the small databases whereas *ARNN+RNN* is unable to deal with the large databases. However, it should be stressed that model size is not the singular explanation for all. Indeed, the unique patterns in case of SHHS (EEG·EOG and EEG·EOG·EMG) seems to be counter-intuitive. As indicated on Section 3.1,

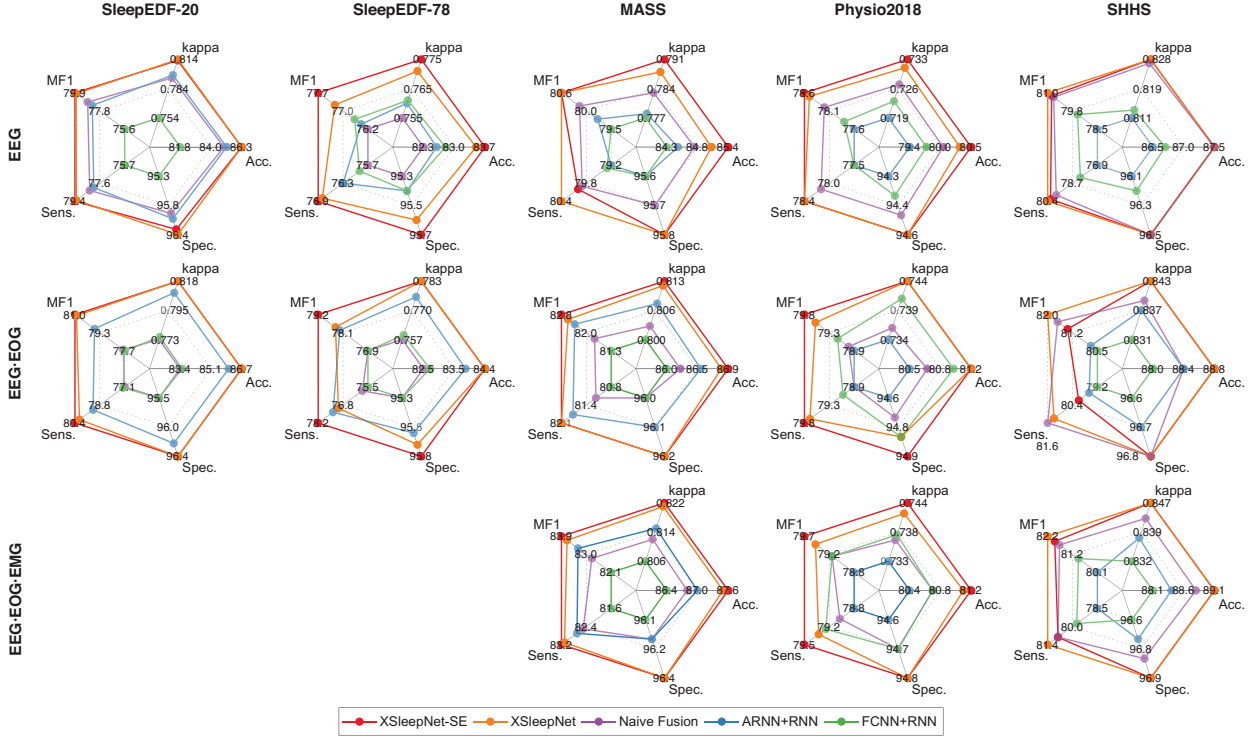


Fig. 3: An overview on the overall performance obtained by XSleepNet, XSleepNet-SE, and the developed baselines.

the CNN-based and RNN-based models tend to capture different kinds of patterns from their input; therefore, performance discrepancies are expected on different sleep stages [10], [50]. This suggests that how well an individual model performs also depends on sleep structure of a target cohort and/or the channel combination used.

Second, simple concatenation of the two views in *Naive Fusion* leads to different, potentially diverging results. One can observe clear performance improvements over the two single-view baselines in some cases, such as MASS (EEG) and Physio2018 (EEG). In some other cases, such as MASS (EEG-EOG) and Physio2018 (EEG-EOG), *Naive Fusion*'s performance appears to be averaged between the two single-view baselines. There are a few extreme cases where *Naive Fusion* is inferior to both single-view baselines, such as in SleepEDF-78 (EEG). These diverging patterns indicate that a naive fusion strategy cannot guarantee performance gain, owing to the asynchronous learning behavior of the two views.

Third, via the generalization-/overfitting-aware learning scheme, the proposed XSleepNet can concert the learning pace of the views, consolidate the representation power of the views in the joint representation, and convert them into performance gains. Improvement over both the single-view and the naive fusion baselines is consistently seen across all the experimental databases and channel combinations. Leveraging self-ensemble of multiple classification outputs, XSleepNet-SE further boosts the performance in many cases, particularly when the data size is small. This result is expected as combining multiple high-variance "models" (due to overfitting effect on small data), we are able to obtain an ensemble model with lower bias than any individual ones [54].

In Table 2, we further lay out the performance detail of the proposed XSleepNet, XSleepNet-SE, and the developed baselines and provide a comprehensive comparison to existing work that used the experimental databases. Particularly, for SleepEDF-20 and SleepEDF-78, we experimented with two common ways these databases were used in literature: (1) only *in-bed* parts of the recordings were used as recommended in [55], [56]; (2) 30 minutes of data before and after *in-bed* parts were further included in the experiments following the initiation in [22].

On the one hand, the results in Table 2 indicate that the single-view baselines developed in this work are competent models for sleep staging. The rationale is that they all adhere to the state-of-the-art sequence-to-sequence sleep staging framework [10], [50]. Under a similar experimental condition, ARNN+RNN outperforms all the existing work across all the scenarios, except U-time [49] on SleepEDF-20. Although the other single-view baseline, FCNN+RNN, underperforms on the smallest database, SleepEDF-20, owing to its large model footprint, its performance improves when the data size increases. The improved result is comparable to, if not better, than those of prior work. On the other hand, the results in Table 2 confirm the efficacy of the proposed XSleepNet. Its performance is not only better than that of the baselines but also superior to that of prior work across all the databases and channel combinations. On average, XSleepNet improves the overall accuracy by 1.1%, 0.7%, and 1.3% absolute over the *Naive Fusion*, ARNN+RNN, and FCNN+RNN baselines, respectively. The corresponding accuracy gains are even higher with XSleepNet-SE when self-ensemble is included, reaching 1.2%, 0.8%, and 1.4%, respectively. Although we do not compute such a performance gain over previous work covered in Table 2 due to

TABLE 2: Performance comparison between the proposed XSleepNet, XSleepNet-SE, the developed baselines, and previous works on the experimental databases. Of note, the ARNN+RNN baseline is equivalent to SeqSleepNet presented in [10]. In addition, the results indicated by \dagger are not directly comparable since they either relied on transfer learning with a pretrained model or used a different subset of the corresponding databases. We include them here for the sake of completeness.

Database	System	EEG					EEG-EOG					EEG-EOG-EMG				
		Acc.	κ	MF1	Sens.	Spec.	Acc.	κ	MF1	Sens.	Spec.	Acc.	κ	MF1	Sens.	Spec.
SleepEDF-20 (± 30 mins)	XSleepNet-SE	86.3	0.813	79.9	79.4	96.3	86.7	0.818	81.0	80.4	96.4	—	—	—	—	—
	XSleepNet	86.3	0.814	79.8	79.3	96.4	86.7	0.818	80.9	80.1	96.4	—	—	—	—	—
	Naive Fusion	<i>85.0</i>	<i>0.795</i>	<i>78.8</i>	<i>78.3</i>	<i>96.0</i>	<i>83.4</i>	<i>0.773</i>	<i>77.8</i>	<i>77.1</i>	<i>95.5</i>	—	—	—	—	—
	ARNN+RNN (SeqSleepNet [10])	<i>85.2</i>	<i>0.798</i>	<i>78.4</i>	<i>78.0</i>	<i>96.1</i>	<i>86.0</i>	<i>0.809</i>	<i>79.7</i>	<i>79.2</i>	<i>96.2</i>	—	—	—	—	—
	FCNN+RNN	<i>81.8</i>	<i>0.754</i>	<i>75.6</i>	<i>75.7</i>	<i>95.3</i>	<i>83.5</i>	<i>0.775</i>	<i>77.7</i>	<i>77.2</i>	<i>95.5</i>	—	—	—	—	—
	DeepSleepNet [22]	—	—	—	—	—	82.0	0.760	76.9	—	—	—	—	—	—	—
	U-time [49]	—	—	79.0	—	—	—	—	—	—	—	—	—	—	—	—
	IITNet [28]	83.9	0.780	77.6	—	—	—	—	—	—	—	—	—	—	—	—
	SeqSleepNet+ \dagger [50]	—	—	—	—	—	—	—	—	—	—	—	—	—	—	—
SleepEDF-20	XSleepNet-SE	83.4	0.765	77.3	77.3	95.4	83.0	0.756	76.8	75.7	95.0	—	—	—	—	—
	XSleepNet	83.0	0.760	76.6	76.6	95.3	82.7	0.752	76.5	75.5	95.0	—	—	—	—	—
	Naive Fusion	<i>80.2</i>	<i>0.723</i>	<i>74.9</i>	<i>75.8</i>	<i>94.7</i>	<i>80.8</i>	<i>0.726</i>	<i>74.7</i>	<i>73.7</i>	<i>94.5</i>	—	—	—	—	—
	ARNN+RNN (SeqSleepNet [10])	<i>82.2</i>	<i>0.746</i>	<i>74.1</i>	<i>73.9</i>	<i>95.0</i>	<i>82.2</i>	<i>0.744</i>	<i>74.2</i>	<i>73.1</i>	<i>94.8</i>	—	—	—	—	—
	FCNN+RNN	<i>81.3</i>	<i>0.737</i>	<i>76.0</i>	<i>76.7</i>	<i>95.0</i>	<i>80.1</i>	<i>0.716</i>	<i>73.2</i>	<i>72.6</i>	<i>94.4</i>	—	—	—	—	—
	Multitask CNN [21]	81.9	0.740	73.8	—	—	82.3	0.750	74.7	—	—	—	—	—	—	—
	DeepSleepNet [22], [50]	80.8	0.731	74.2	—	—	81.9	0.744	75.2	—	—	—	—	—	—	—
	1-max CNN [18]	79.8	0.720	72.0	—	—	—	—	—	—	—	—	—	—	—	—
	Attentional RNN [19]	79.1	0.700	69.8	—	—	—	—	—	—	—	—	—	—	—	—
	Auto-encoder [23]	78.9	—	73.3	—	—	—	—	—	—	—	—	—	—	—	—
	ResNet [25]	—	0.650	—	—	—	—	0.680	—	—	—	—	—	—	—	—
	VGG-FE [51]	76.3	—	—	—	—	—	—	—	—	—	—	—	—	—	—
	CNN [17]	74.8	—	69.8	—	—	—	—	—	—	—	—	—	—	—	—
	FT SeqSleepNet+ \dagger [50]	85.2	0.789	79.6	—	—	84.3	0.776	77.7	—	—	—	—	—	—	—
	FT DeepSleepNet+ \dagger [50]	84.4	0.781	78.8	—	—	84.6	0.782	79.0	—	—	—	—	—	—	—
	Person CNN \dagger [27]	84.0	—	—	—	—	—	—	—	—	—	—	—	—	—	—
	VGG-FT \dagger [51]	80.3	—	—	—	—	—	—	—	—	—	—	—	—	—	—
SleepEDF-78 (± 30 mins)	XSleepNet-SE	83.7	0.775	77.7	76.9	95.7	84.4	0.783	79.2	78.2	95.8	—	—	—	—	—
	XSleepNet	83.5	0.771	77.2	76.8	95.6	84.4	0.783	78.4	77.1	95.7	—	—	—	—	—
	Naive Fusion	<i>82.3</i>	<i>0.755</i>	<i>76.2</i>	<i>75.7</i>	<i>95.3</i>	<i>82.5</i>	<i>0.757</i>	<i>76.9</i>	<i>75.8</i>	<i>95.3</i>	—	—	—	—	—
	ARNN+RNN (SeqSleepNet [10])	<i>82.6</i>	<i>0.760</i>	<i>76.4</i>	<i>76.3</i>	<i>95.4</i>	<i>83.8</i>	<i>0.776</i>	<i>78.2</i>	<i>77.4</i>	<i>95.6</i>	—	—	—	—	—
	FCNN+RNN	<i>82.8</i>	<i>0.761</i>	<i>76.6</i>	<i>75.9</i>	<i>95.4</i>	<i>82.7</i>	<i>0.759</i>	<i>76.9</i>	<i>75.5</i>	<i>95.3</i>	—	—	—	—	—
	U-Time [49]	—	—	76.0	—	—	—	—	—	—	—	—	—	—	—	—
	CNN-LSTM [49]	—	—	73.0	—	—	—	—	—	—	—	—	—	—	—	—
	SleepEEGNet [52]	80.0	0.730	73.6	—	—	—	—	—	—	—	—	—	—	—	—
	SeqSleepNet+ \dagger [50]	—	—	—	—	—	—	—	—	—	—	—	—	—	—	—
SleepEDF-78	XSleepNet-SE	80.0	0.722	76.3	75.9	94.5	80.8	0.732	77.0	75.8	94.5	—	—	—	—	—
	XSleepNet	80.1	0.723	76.2	75.5	94.5	80.9	0.732	76.8	75.9	94.6	—	—	—	—	—
	Naive Fusion	<i>79.1</i>	<i>0.709</i>	<i>75.1</i>	<i>74.3</i>	<i>94.2</i>	<i>79.3</i>	<i>0.711</i>	<i>75.7</i>	<i>74.2</i>	<i>94.1</i>	—	—	—	—	—
	ARNN+RNN (SeqSleepNet [10])	<i>79.0</i>	<i>0.708</i>	<i>74.6</i>	<i>74.2</i>	<i>94.2</i>	<i>79.7</i>	<i>0.715</i>	<i>75.7</i>	<i>74.6</i>	<i>94.2</i>	—	—	—	—	—
	FCNN+RNN	<i>79.3</i>	<i>0.711</i>	<i>75.1</i>	<i>74.0</i>	<i>94.2</i>	<i>79.8</i>	<i>0.717</i>	<i>76.1</i>	<i>74.9</i>	<i>94.3</i>	—	—	—	—	—
	Personalized SeqSleepNet \dagger [53]	79.6	0.706	73.0	71.8	94.2	—	—	—	—	—	—	—	—	—	—
	DeepSleepNet [22], [53]	78.5	0.702	75.3	75.0	94.1	—	—	—	—	—	—	—	—	—	—
	SeqSleepNet+ \dagger [50]	—	—	—	—	—	—	—	—	—	—	—	—	—	—	—
	SeqSleepNet+ \dagger [50]	—	—	—	—	—	—	—	—	—	—	—	—	—	—	—
MASS	XSleepNet-SE	85.4	0.791	80.6	80.0	95.8	86.9	0.813	82.8	82.1	96.2	87.6	0.822	83.9	83.2	96.4
	XSleepNet	85.1	0.788	80.6	80.4	95.8	86.8	0.812	82.6	82.1	96.2	87.5	0.821	83.7	83.1	96.4
	Naive Fusion	<i>84.8</i>	<i>0.783</i>	<i>80.2</i>	<i>79.9</i>	<i>95.7</i>	<i>86.2</i>	<i>0.803</i>	<i>81.8</i>	<i>81.2</i>	<i>96.0</i>	<i>86.8</i>	<i>0.812</i>	<i>82.8</i>	<i>82.5</i>	<i>96.2</i>
	ARNN+RNN (SeqSleepNet [10])	<i>84.5</i>	<i>0.778</i>	<i>79.8</i>	<i>79.2</i>	<i>95.6</i>	<i>86.5</i>	<i>0.808</i>	<i>82.4</i>	<i>81.8</i>	<i>96.1</i>	<i>87.0</i>	<i>0.815</i>	<i>83.3</i>	<i>82.7</i>	<i>96.2</i>
	FCNN+RNN	<i>84.3</i>	<i>0.777</i>	<i>79.5</i>	<i>79.3</i>	<i>95.6</i>	<i>86.0</i>	<i>0.800</i>	<i>81.3</i>	<i>80.8</i>	<i>96.0</i>	<i>86.4</i>	<i>0.806</i>	<i>82.1</i>	<i>81.6</i>	<i>96.1</i>
	DeepSleepNet [10], [22]	—	—	—	—	—	—	—	—	—	—	—	—	—	—	—
	Multitask CNN [10], [21]	—	—	—	—	—	—	—	—	—	—	—	—	—	—	—
	Attentional RNN [10], [19]	—	—	—	—	—	—	—	—	—	—	—	—	—	—	—
	1-max CNN [10], [18]	—	—	—	—	—	—	—	—	—	—	—	—	—	—	—
	CNN [10], [20]	—	—	—	—	—	—	—	—	—	—	—	—	—	—	—
	CNN [10], [17]	—	—	—	—	—	—	—	—	—	—	—	—	—	—	—
	ResNet [25]	—	0.670	—	—	—	—	0.720	—	—	—	—	—	—	—	—
	IITNet \dagger [28]	86.3	0.790	80.5	—	—	—	—	—	—	—	—	—	—	—	—
Physio2018	XSleepNet-SE	80.5	0.733	78.6	78.4	94.6	81.2	0.744	79.8	79.8	94.9	81.2	0.744	79.7	79.5	94.8
	XSleepNet	80.3	0.731	78.5	78.4	94.6	81.2	0.744	79.6	79.7	94.8	81.1	0.742	79.5	79.3	94.8
	Naive Fusion	<i>80.0</i>	<i>0.727</i>	<i>78.2</i>	<i>78.1</i>	<i>94.5</i>	<i>80.7</i>	<i>0.736</i>	<i>79.0</i>	<i>78.9</i>	<i>94.7</i>	<i>80.7</i>	<i>0.737</i>	<i>79.2</i>	<i>79.0</i>	<i>94.7</i>
	ARNN+RNN (SeqSleepNet [10])	<i>79.4</i>	<i>0.719</i>	<i>77.6</i>	<i>77.5</i>	<i>94.3</i>	<i>80.5</i>	<i>0.734</i>	<i>78.9</i>	<i>78.9</i>	<i>94.6</i>	<i>80.4</i>	<i>0.733</i>	<i>78.8</i>	<i>78.8</i>	<i>94.6</i>
	FCNN+RNN	<i>79.7</i>	<i>0.723</i>	<i>77.8</i>	<i>77.5</i>	<i>94.4</i>	<i>81.0</i>	<i>0.741</i>	<i>79.2</i>	<i>79.1</i>	<i>94.8</i>	<i>80.7</i>	<i>0.738</i>	<i>79.2</i>	<i>79.2</i>	<i>94.7</i>
	U-Time [49]	—	—	77.0	—	—	—	—	—	—	—	—	—	77.0	—	—
	CNN-LSTM [49]	—	—	77.0	—	—	—	—	—	—	—	—	—	—	—	—
SHHS	XSleepNet-SE	87.5	0.826	80.8	80.2	96.5	88.8	0.843	81.4	80.1	96.8	89.1	0.847	81.9	80.8	96.9
	XSleepNet	87.5	0.826	81.0	80.4	96.5	88.8	<								

TABLE 3: Class-wise performance of the proposed XSleepNet, XSleepNet-SE, and the developed baselines in terms of MF1.

Database	System	EEG					EEG·EOG					EEG·EOG·EMG				
		W	N1	N2	N3	REM	W	N1	N2	N3	REM	W	N1	N2	N3	REM
SleepEDF-20 (± 30 mins)	XSleepNet-SE	92.0	48.2	88.1	86.7	84.5	92.0	51.4	87.8	86.8	87.2	—	—	—	—	—
	XSleepNet	91.7	47.5	88.3	87.3	84.4	91.5	50.1	87.8	87.1	87.8	—	—	—	—	—
	Naive Fusion	91.7	48.8	87.2	82.9	83.6	88.6	46.9	85.3	84.2	83.7	—	—	—	—	—
	ARNN+RNN	90.5	45.4	88.1	86.4	81.8	91.9	47.8	87.2	85.7	86.2	—	—	—	—	—
	FCNN+RNN	89.4	44.1	84.0	84.0	76.3	87.7	45.8	86.3	84.7	84.0	—	—	—	—	—
SleepEDF-20	XSleepNet-SE	79.9	47.6	88.3	86.7	83.8	74.3	48.5	87.0	86.9	87.4	—	—	—	—	—
	XSleepNet	78.6	46.4	87.9	86.1	84.1	73.1	48.4	86.9	86.9	87.0	—	—	—	—	—
	Naive Fusion	77.3	47.4	85.8	84.8	79.3	72.2	46.3	85.8	84.6	84.4	—	—	—	—	—
	ARNN+RNN	78.5	37.1	87.6	86.2	81.2	75.0	38.3	86.8	86.0	85.0	—	—	—	—	—
	FCNN+RNN	76.4	50.0	86.8	85.3	81.3	66.7	44.2	86.0	84.8	84.4	—	—	—	—	—
SleepEDF-78 (± 30 mins)	XSleepNet-SE	93.0	49.5	85.8	78.3	81.8	92.8	50.5	85.6	80.2	86.6	—	—	—	—	—
	XSleepNet	92.6	47.7	85.8	79.1	80.6	92.8	48.2	86.0	79.0	86.1	—	—	—	—	—
	Naive Fusion	93.2	49.6	86.2	79.4	82.5	91.0	47.7	84.7	77.7	83.6	—	—	—	—	—
	ARNN+RNN	92.2	47.8	84.9	77.2	79.9	92.8	48.9	85.4	78.6	85.1	—	—	—	—	—
	FCNN+RNN	92.5	47.3	85.0	79.2	78.9	91.2	45.8	84.7	78.5	84.2	—	—	—	—	—
SleepEDF-78	XSleepNet-SE	85.3	50.7	85.5	79.3	80.7	84.7	49.5	85.9	79.0	86.0	—	—	—	—	—
	XSleepNet	84.9	50.6	85.8	78.9	81.0	85.1	48.0	86.1	79.4	85.5	—	—	—	—	—
	Naive Fusion	83.9	47.8	85.4	78.4	79.8	82.1	49.8	85.2	77.5	83.8	—	—	—	—	—
	ARNN+RNN	83.2	46.8	85.5	76.3	81.0	83.7	47.3	85.2	77.6	84.5	—	—	—	—	—
	FCNN+RNN	84.2	49.1	85.2	76.8	80.4	83.4	49.1	85.0	78.0	84.8	—	—	—	—	—
MASS	XSleepNet-SE	87.3	56.8	89.4	82.5	87.1	89.3	60.9	90.3	82.8	90.8	90.5	63.6	90.3	82.8	92.3
	XSleepNet	87.1	58.0	89.2	82.1	86.7	88.7	59.9	90.2	83.1	91.0	90.0	62.8	90.4	82.9	92.3
	Naive Fusion	87.0	56.6	89.0	81.6	86.5	88.4	58.5	89.8	82.3	90.1	89.4	61.1	89.9	82.4	91.3
	ARNN+RNN	87.3	55.3	88.7	81.7	86.1	89.3	60.2	89.8	82.0	90.8	89.8	62.7	89.9	82.4	91.9
	FCNN+RNN	86.0	55.5	88.8	82.1	85.3	87.5	56.3	89.8	83.1	90.1	88.1	59.0	89.8	83.0	90.8
Physio2018	XSleepNet-SE	83.8	59.0	85.0	79.7	85.4	84.5	60.3	85.1	80.7	88.1	84.4	60.4	85.2	80.3	88.1
	XSleepNet	83.9	58.6	84.7	79.9	85.3	84.5	60.0	85.1	80.3	88.2	84.4	60.3	85.0	79.7	88.3
	Naive Fusion	83.4	58.9	84.5	79.8	84.6	84.0	59.2	84.8	79.4	87.7	83.8	59.5	84.8	79.8	87.9
	ARNN+RNN	82.6	58.6	83.9	79.3	83.6	84.0	59.8	84.4	79.2	87.3	83.6	58.9	84.5	79.8	87.3
	FCNN+RNN	83.2	57.8	84.5	79.3	84.1	84.1	58.8	85.2	80.3	87.7	83.8	59.5	84.8	79.9	87.9
SHHS	XSleepNet-SE	91.7	50.7	88.5	85.1	88.1	93.0	48.2	89.4	85.3	91.2	93.4	49.4	89.6	85.5	91.7
	XSleepNet	91.6	51.4	88.5	85.0	89.3	93.4	51.0	89.4	84.9	91.3	93.5	50.5	89.5	85.7	91.6
	Naive Fusion	91.9	50.9	88.4	84.1	88.3	93.0	50.9	89.2	85.2	90.2	93.2	49.6	89.3	85.3	91.3
	ARNN+RNN	91.4	43.3	87.4	82.9	87.3	93.1	46.2	88.9	84.7	90.8	93.3	42.6	88.8	84.3	91.5
	FCNN+RNN	91.1	48.7	88.0	82.6	87.1	92.3	47.0	88.7	84.3	90.4	92.5	48.5	88.8	84.3	90.5

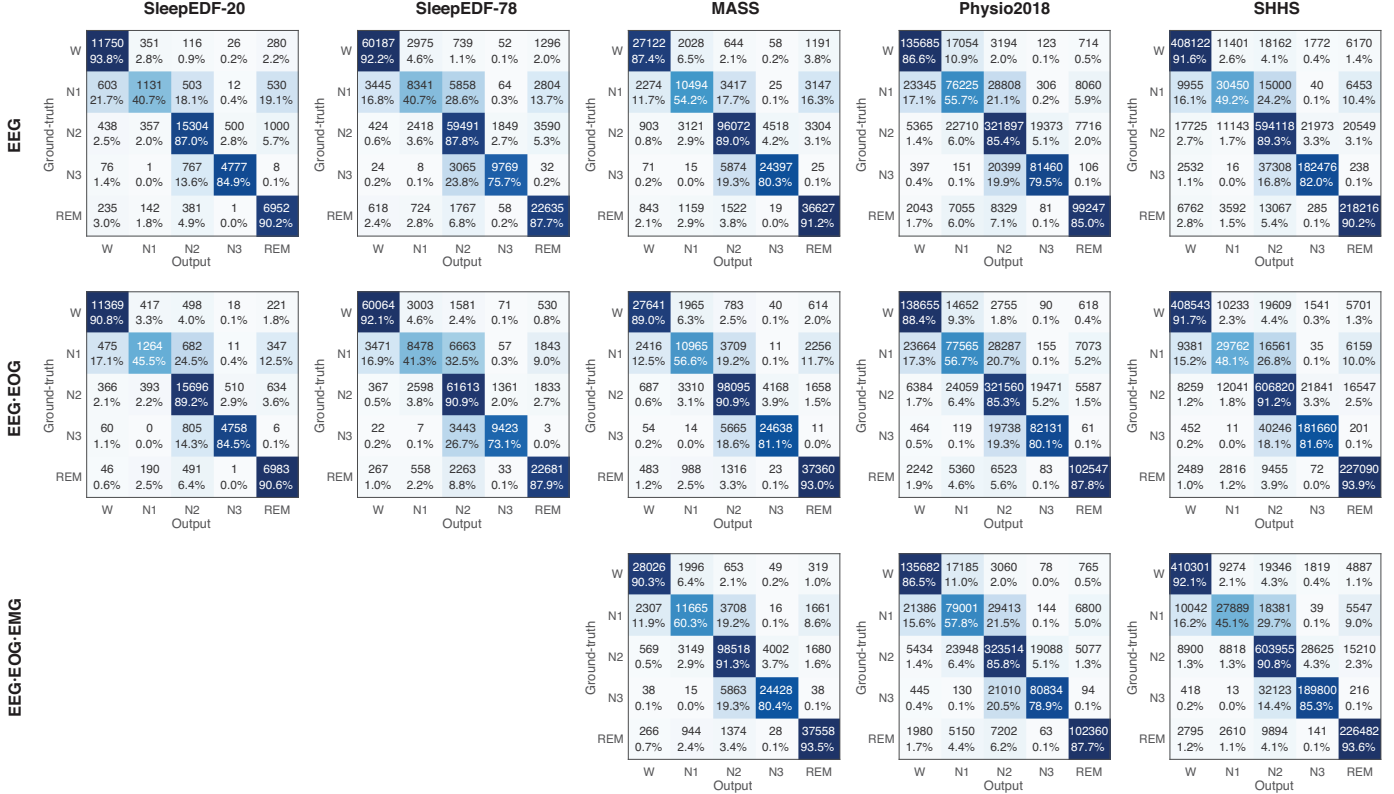


Fig. 4: Confusion matrices obtained by XSleepNet for the experimental databases and channel combinations.

their incomplete reported results, improvement with a large margin can be expected.

The complete class-wise performance obtained by XSleepNet, XSleepNet-SE, and the baselines in terms of MF1 are further shown in Table 3. On the one hand, one can see with many databases and channel combinations that ARNN+RNN and FCNN+RNN often favor different sleep stages. For example, on MASS (EEG-EOG-EMG), the former outperforms the latter on N1 whereas the latter is better than the former on N3, confirming the similar finding in [10]. However, it should be noted that the sleep stage favorability of the two baselines varies from one database to another. We conjecture that this property is cohort-dependent. On the other hand, with simple concatenation fusion, the *Naive Fusion* baseline results in class-wise MF1 lying between that of ARNN+RNN and that of FCNN+RNN in most of the cases, reflecting its averaging learning behavior (cf. Fig. 1). In contrast, improvements on class-wise MF1 are expectedly seen with XSleepNet, XSleepNet-SE. More importantly, most of the time these improvements are spread over the five sleep stages rather than biasing towards some particular ones. One may also notice the particular poor performance on N1 of all the sleep staging models, including XSleepNet and XSleepNet-SE. This is not because of model deficiencies but the human sleep structure itself. It is well-known in sleep research that N1, which is the transitioning stage between Wake and N2, occurs right after one falls asleep and is very short (usually less than 10 minutes) [7], [8], [57]. As a result, correctly recognizing N1 is challenging partly due to its limited occurrence and partly due to its similarity to Wake and N2 as revealed by XSleepNet’s confusion matrices in Fig. 4.

5 DISCUSSION

To see how the loss weights were adapted for gradient blending during the training course of XSleepNet, we take one cross-validation fold of the MASS database as an example, which is illustrated in Fig. 5. In case of the single-view training with ARNN+RNN and FCNN+RNN, even though the former’s validation loss did not show signs of overfitting, the latter with a large model footprint converged and started overfitting after 10^5 training steps (cf. Fig. 5 (a)). As a consequence, when the two views were trained jointly with a simple fusion strategy in *Naive Fusion*, the overfitting network stream kept learning at the same rate, deteriorating the joint-view representation and causing overfitting (even though less serious) in the joint classification branch (it can be roughly thought as being the average of the two views). In contrast, during training of XSleepNet (cf. Fig. 5 (b) and (c)), the view in red that was converging faster was initially associated with an increasingly large weight while a small weight was assigned to the one in blue (the slower one). Note that the latter view was still able to learn due to the gradient flow coming from the joint classification branch (the green curve). The turning point was when the view in red converged and started overfitting shortly after that, its weights descended, impeding its learning and, hence, preventing it from overfitting the data at the regular pace. On the other hand, the weight that the view in red lost was transferred to the view in blue to accelerate its

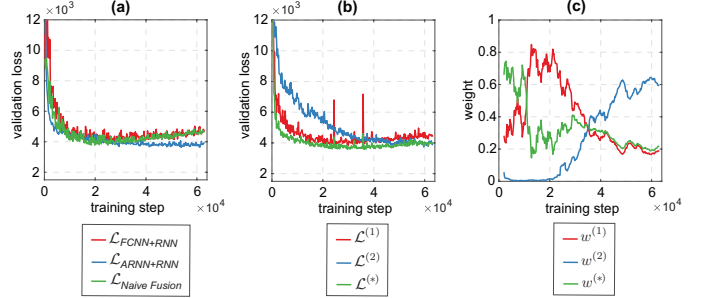


Fig. 5: Progression of the validation losses and the adaptive loss weights during the training course of one MASS cross-validation fold. (a) The validation losses of the FCNN+RNN, ARNN+RNN, and *Naive Fusion* baselines; (b) The validation losses of the three classification branches of XSleepNet; (c) The adaptive loss weights computed for the three classification branches of XSleepNet. Note that the adaptive loss weights were denoised with a 10-point average moving filter before plotting.

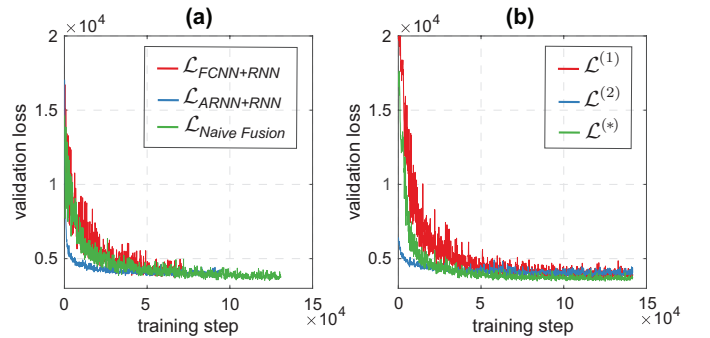


Fig. 6: The validation losses during the training course of the SHHS database. (a) The validation losses of the FCNN+RNN, ARNN+RNN, and *Naive Fusion* baselines; (b) The validation losses of the three classification branches of XSleepNet.

learning. As a result, the joint learning process yields the joint representation which is more robust to overfitting and more generalizable than those learned by the *Naive Fusion* baseline.

Out of five experimental databases, only on SHHS, the largest database, did we see similar behavior between the *Naive Fusion* and the proposed XSleepNet. In other words, the *Naive Fusion* model resulted in consistently better results than the single-view baselines (cf. Fig. 3 and Table 2). The reason is when the data becomes large enough, it imposes a strong regularization on network. As a consequence, the networks, either in single-view training or in joint training, did not experience overfitting as with smaller databases, as evidenced by the validation losses in Fig. 5. We anticipate that the model capacity can be safely increased in this case.

It is worth mentioning that even though XSleepNet has two network streams, its model footprint (5.8×10^6 parameters) is still 4 times smaller than the popular Deep-SleepNet (22.9×10^6 parameters). In addition, although we experimented the proposed XSleepNet on automatic sleep staging with PSG signals, the method is generic enough

to serve sleep analysis with other modalities, especially when multimodal data are available [58], [59]. It is also applicable to other applications where the target signals are inherently multi-view. One example is audio/speech in which raw audio signals [60] can be combined with its derived representations, such as mel-scale spectrogram [61] and gammatone spectrogram [62], for recognition tasks. Another example is computer vision in which different image channels, such as luminance, chrominance, depth, and optical flow, are essentially multi-view data [30], [63].

6 CONCLUSIONS

In this paper, we presented XSleepNet, a sequence-to-sequence sleep staging model, that is capable of learning from both raw signal and time-frequency input at the same time. The network accommodates two network streams, one for each input view. XSleepNet is principally designed to gain robustness to training data size, complementarity between the constituent network streams, and awareness of generalization and overfitting behavior of its network stream. The network can be trained in such a way that learning on the generalizing network stream is encouraged while that on the overfitting one is discouraged. By adaptively regulating the learning pace of the network streams, XSleepNet yielded joint features which represent the underlying data distribution better than those learned by the single-view baselines as well as the multi-view baseline following a naive fusion approach. Empirical evaluation showed that XSleepNet not only delivered more favorable results than the baselines but also significantly outperformed existing work on five databases of different sizes.

ACKNOWLEDGMENTS

The authors would like to acknowledge and thank Dr. Long Tran-Thanh, University of Warwick, for his helpful discussion and comments.

REFERENCES

- [1] P. Maquet, "The role of sleep in learning and memory," *Science*, vol. 294, no. 5544, pp. 1048–1052, 2001.
- [2] A. C. Krieger, Ed., *Social and Economic Dimensions of Sleep Disorders, An Issue of Sleep Medicine Clinics*, Elsevier, 2017.
- [3] V. K. Chatta, D. Manzar, S. Kumary, D. Burman, D. W. Spence, and S. R. Pandi-Perumal, "The global problem of insufficient sleep and its serious public health implications," in *Healthcare (Basel)*, 2019, vol. 7.
- [4] Institute of Medicine, *Sleep Disorders and Sleep Deprivation: An Unmet Public Health Problem*, Washington DC: The National Academies Press, 2006.
- [5] K. B. Mikkelsen, J. K. Ebajemito, M. A. BonmatiCarrión, N. Santhi, V. L. Revell, G. Atzori, C. della Monica, S. Debener, D. J. Dijk, A. Sterr, and M. de Vos, "Machinelearningderived sleepwake staging from aroundtheear electroencephalogram outperforms manual scoring and actigraphy," *Journal of Sleep Research*, vol. 28, no. 2, pp. e12786, 2019.
- [6] K. B. Mikkelsen *et al.*, "Accurate whole-night sleep monitoring with dry-contact ear-EEG," *Scientific reports*, vol. 9, no. 1, pp. 1–12, 2019.
- [7] C. Iber, S. Ancoli-Israel, A. L. Chesson, and S. F. Quan, "The AASM manual for the scoring of sleep and associated events: Rules, terminology and technical specifications," *American Academy of Sleep Medicine*, 2007.
- [8] J. A. Hobson, "A manual of standardized terminology, techniques and scoring system for sleep stages of human subjects," *Electroencephalography and Clinical Neurophysiology*, vol. 26, no. 6, pp. 644–649, 1969.
- [9] A. Malhotra, M. Younes, S. T. Kuna, R. Bencs, C. A. Kushida, J. Walsh, A. Hanlon, B. Staley, A. I. Pack, and G. W. Pien, "Performance of an automated polysomnography scoring system versus computer-assisted manual scoring," *SLEEP*, vol. 36, no. 4, pp. 573–582, 2013.
- [10] H. Phan, F. Andreotti, N. Cooray, O. Y. Chén, and M. De Vos, "SeqSleepNet: end-to-end hierarchical recurrent neural network for sequence-to-sequence automatic sleep staging," *IEEE Transactions on Neural Systems and Rehabilitation Engineering (TNSRE)*, vol. 27, no. 3, pp. 400–410, 2019.
- [11] J. B. Stephansen, A. N. Olesen, M. Olsen, A. Ambati, E. B. Leary, H. E. Moore, O. Carrillo, L. Lin, F. Han, H. Yan, Y. L. Sun, Y. Dauvilliers, S. Scholz, L. Barateau, B. Hogl, A. Stefani, S. C. Hong, T. W. Kim, F. Pizza, G. Plazzi, S. Vandi, E. Antelmi, D. Perrin, S. T. Kuna, P. K. Schweitzer, C. Kushida, P. E. Peppard, H. B. D. Sorensen, P. Jennm, and E. Mignot, "Neural network analysis of sleep stages enables efficient diagnosis of narcolepsy," *Nature Communications*, vol. 9, no. 1, pp. 5229, 2018.
- [12] C. O'Reilly, N. Gosselin, J. Carrier, and T. Nielsen, "Montreal archive of sleep studies: An open-access resource for instrument benchmarking & exploratory research," *Journal of Sleep Research*, pp. 628–635, 2014.
- [13] S. Biswal, H. Sun, B. Goparaju, M. B. Westover, J. Sun, and M. T. Bianchi, "Expert-level sleep scoring with deep neural networks," *J Am Med Inform Assoc.*, 2018.
- [14] S. Biswal, J. Kulas, H. Sun, B. Goparaju, M. B. Westover, M. T. Bianchi, and J. Sun, "SLEEPNET: Automated sleep staging system via deep learning," *arXiv preprint arXiv:1707.08262*, 2017.
- [15] H. Sun, J. Jia, B. Goparaju, G.-B. Huang, O. Sourina, M. T. Bianchi, and M. B. Westover, "Large-scale automated sleep staging," *SLEEP*, vol. 40, no. 10, pp. zsx139, 2017.
- [16] M. Längkvist, L. Karlsson, and A. Loutfi, "Sleep stage classification using unsupervised feature learning," *Advances in Artificial Neural Systems*, vol. 2012, pp. 1–9, 2012.
- [17] O. Tsinalis, P. M. Matthews, Y. Guo, and S. Zafeiriou, "Automatic sleep stage scoring with single-channel EEG using convolutional neural networks," *arXiv preprint arXiv:1610.01683*, 2016.
- [18] H. Phan, F. Andreotti, N. Cooray, O. Y. Chén, and M. De Vos, "DNN filter bank improves 1-max pooling CNN for single-channel EEG automatic sleep stage classification," in *Proc. EMBC*, 2018, pp. 453–456.
- [19] H. Phan, F. Andreotti, N. Cooray, O. Y. Chén, and M. De Vos, "Automatic sleep stage classification using single-channel eeg: Learning sequential features with attention-based recurrent neural networks," in *Proc. EMBC*, 2018, pp. 1452–1455.
- [20] S. Chambon, M. N. Galtier, P. J. Arnal, G. Wainrib, and A. Gramfort, "A deep learning architecture for temporal sleep stage classification using multivariate and multimodal time series," *IEEE Trans. on Neural Systems and Rehabilitation Engineering*, vol. 26, no. 4, pp. 758–769, 2018.
- [21] H. Phan, F. Andreotti, N. Cooray, O. Y. Chén, and M. De Vos, "Joint classification and prediction CNN framework for automatic sleep stage classification," *IEEE Transactions Biomedical Engineering (TBME)*, vol. 66, no. 5, pp. 1285–1296, 2019.
- [22] A. Supratak, H. Dong, C. Wu, and Y. Guo, "DeepSleepNet: A model for automatic sleep stage scoring based on raw single-channel EEG," *IEEE Trans. on Neural Systems and Rehabilitation Engineering*, vol. 25, no. 11, pp. 1998–2008, 2017.
- [23] O. Tsinalis, P. M. Matthews, and Y. Guo, "Automatic sleep stage scoring using time-frequency analysis and stacked sparse autoencoders," *Annals of Biomedical Engineering*, vol. 44, no. 5, pp. 1587–1597, 2016.
- [24] H. Dong, A. Supratak, W. Pan, C. Wu, P. M. Matthews, and Y. Guo, "Mixed neural network approach for temporal sleep stage classification," *IEEE Trans. on Neural Systems and Rehabilitation Engineering*, vol. 26, no. 2, pp. 324–333, 2018.
- [25] F. Andreotti, H. Phan, N. Cooray, C. Lo, M. T. M. Hu, and M. De Vos, "Multichannel sleep stage classification and transfer learning using convolutional neural networks," in *Proc. EMBC*, 2018, pp. 171–174.
- [26] A. Sors, S. Bonnet, S. Mirek, L. Vercueil, and J.-F. Payen, "A convolutional neural network for sleep stage scoring from raw

single-channel eeg," *Biomedical Signal Processing and Control*, vol. 42, pp. 107–114, 2018.

[27] K. Mikkelsen and M. De Vos, "Personalizing deep learning models for automatic sleep staging," *arXiv Preprint arXiv:1801.02645*, 2018.

[28] H. Seo, S. Back, S. Lee, D. Park, T. Kim, and K. Lee, "Intra- and inter-epoch temporal context network (iitnet) using sub-epoch features for automatic sleep scoring on raw single-channel eeg," *Biomedical Signal Processing and Control*, 2020.

[29] J. Zhao, X. Xie, X. Xu, and S. Sun, "Multi-view learning overview: Recent progress and new challenges," *Information Fusion*, vol. 38, pp. 43–54, 2017.

[30] X. Chen, H. Ma, J. Wan, B. Li, and T. Xia, "Multi-view 3d object detection network for autonomous driving," in *Proc. CVPR*, 2017, pp. 6526–6534.

[31] A. Tsymbal, M. Pechenizkiy, and P. Cunningham, "Diversity in search strategies for ensemble feature selection," *Information Fusion*, vol. 6, no. 1, pp. 83–98, 2005.

[32] H. Phan, O. Y. Chén, P. Koch, A. Mertins, and M. De Vos, "Fusion of end-to-end deep learning models for sequence-to-sequence sleep staging," in *Proc. EMBC*, 2019.

[33] K. Cho, B. van Merriënboer, C. Gulcehre, F. Bougares, H. Schwenk, and Y. Bengio, "Learning phrase representations using RNN encoder-decoder for statistical machine translation," in *Proc. EMNLP*, 2014, pp. 1724–1734.

[34] S. Hochreiter and J. Schmidhuber, "Long short-term memory," *Neural Computing*, vol. 9, no. 8, pp. 1735–1780, 1997.

[35] T. Cooijmans, N. Ballas, C. Laurent, C. Gülcöhre, and A. Courville, "Recurrent batch normalization," *arXiv Preprint arXiv:1603.09025*, 2016.

[36] J. Long, E. Shelhamer, and T. Darrell, "Fully convolutional networks for semantic segmentation," in *Proc. CVPR*, 2015, number 3431–3440.

[37] K. He, X. Zhang, S. Ren, and J. Sun, "Delving deep into rectifiers: Surpassing human-level performance on imagenet classification," in *Proc. ICCV*, 2015, pp. 1026–1034.

[38] W. Wang, D. Tran, and M. Feiszli, "What makes training multimodal networks hard?," in *Proc. CVPR 2020*, 2020.

[39] B. Kemp, A. H. Zwinderman, B. Tuk, H. A. C. Kamphuisen, and J. J. L. Oberye, "Analysis of a sleep-dependent neuronal feedback loop: the slow-wave microcontinuity of the EEG," *IEEE Trans. on Biomedical Engineering*, vol. 47, no. 9, pp. 1185–1194, 2000.

[40] A. L. Goldberger, L. A. N. Amaral, L. Glass, J. M. Hausdorff, P. Ch. Ivanov, R. G. Mark, J. E. Mietus, G. B. Moody, C.-K. Peng, and H. E. Stanley, "Physiobank, physiotoolkit, and physionet: Components of a new research resource for complex physiologic signals," *Circulation*, vol. 101, pp. e215–e220, 2000.

[41] M. M. Ghassemi, B. E. Moody, L. H. Lehman, C. Song, Q. Li, H. Sun, R. G. Mark, M. B. Westover, and G. D. Clifford, "You snooze, you win: the physionet/computing in cardiology challenge 2018," in *Proc. 2018 Computing in Cardiology Conference (CinC)*, 2018, vol. 45.

[42] G. Q. Zhang, L. Cui, R. Mueller, S. Tao, M. Kim, M. Rueschman, S. Mariani, D. Mobley, and S. Redline, "The national sleep research resource: towards a sleep data commons," *J Am Med Inform Assoc.*, vol. 25, no. 10, pp. 1351–1358, 2018.

[43] S. F. Quan, B. V. Howard, C. Iber, J. P. Kiley, F. J. Nieto, G. T. O'Connor, D. M. Rapoport, S. Redline, J. Robbins, J. M. Samet, and P. W. Wahl, "The sleep heart health study: design, rationale, and methods," *Sleep*, vol. 20, no. 12, pp. 1077–1085, 1997.

[44] M. Abadi *et al.*, "Tensorflow: Large-scale machine learning on heterogeneous distributed systems," *arXiv:1603.04467*, 2016.

[45] N. Srivastava, G. Hinton, A. Krizhevsky, I. Sutskever, and R. Salakhutdinov, "Dropout: A simple way to prevent neural networks from overfitting," *Journal of Machine Learning Research (JMLR)*, vol. 15, pp. 1929–1958, 2014.

[46] D. P. Kingma and J. L. Ba, "Adam: a method for stochastic optimization," in *Proc. ICLR*, 2015, number 1-13.

[47] Y. Yang, , and X. Liu, "A re-examination of text categorization methods," in *Proc. SIGIR*, 1999, vol. 99, pp. 42–49.

[48] M. L. McHugh, "Interrater reliability: the kappa statistic," *Biometria Medica*, 2012.

[49] M. Perslev, M. H. Jensen, S. Darkner, P. J. Jenum, and C. Igel, "U-time: A fully convolutional network for time series segmentation applied to sleep staging," in *Proc. NeurIPS*, 2019, pp. 4417–4428.

[50] H. Phan, O. Y. Chén, P. Koch, Z. Lu, I. McLoughlin, A. Mertins, and M. De Vos, "Towards more accurate automatic sleep staging via deep transfer learning," *arXiv preprint arXiv:1907.13177*, 2019.

[51] Albert Vilamala, Kristoffer H. Madsen, and Lars K. Hansen, "Deep convolutional neural networks for interpretable analysis of EEG sleep stage scoring," in *Proc. MLSP*, 2017.

[52] S. Mousavi, F. Afghah, and R. Acharya, "SleepEEGNet: Automated sleep stage scoring with sequence to sequence deep learning approach," *PLoS One*, vol. 14, no. 5, pp. e0216456, 2019.

[53] H. Phan, K. Mikkelsen, O. Y. Chén, P. Koch, A. Mertins, P. Kidmose, and M. De Vos, "Personalized automatic sleep staging with single-night data: a pilot study with KL-divergence regularization," *Physiological Measurement*, vol. 41, no. 6, pp. 064004, 2020.

[54] S. Dzeroski and B. Zenko, "Is combining classifiers with stacking better than selecting the best one?," *Machine Learning*, vol. 54, no. 3, pp. 255–273, 2004.

[55] S. A. Imtiaz and E. Rodriguez-Villegas, "Recommendations for performance assessment of automatic sleep staging algorithms," in *Proc. EMBC*, 2014, pp. 5044–5047.

[56] S. A. Imtiaz and E. Rodriguez-Villegas, "An open-source toolbox for standardized use of PhysioNet Sleep EDF Expanded Database," in *Proc. EMBC*, 2015, pp. 6014–6017.

[57] R. K. Malhotra and A. Y. Avidan, *Atlas of Clinical Sleep Medicine*, chapter Sleep Stages and Scoring Technique, Saunders/Elsevier, 2014.

[58] B. Zhai, I. Perez-Pozuelo, E. A. D. Clifton, J. Palotti, and Y. Guan, "Making sense of sleep: Multimodal sleep stage classification in a large, diverse population using movement and cardiac sensing," in *Proc. ACM Interact. Mob. Wearable Ubiquitous Technol.*, 2020, vol. 4.

[59] A. N. Olesen, S. Chambon, V. Thorey, P. Jenum, E. Mignot, and H. B. D. Sorensen, "Towards a flexible deep learning method for automatic detection of clinically relevant multi-modal events in the polysomnogram," in *Proc. EMBC*, 2019, pp. 556–561.

[60] D. Palaz, M. Magimai-Doss, and R. Collobert, "Convolutional neural networks-based continuous speech recognition using raw speech signal," in *Proc. ICASSP*, 2015, pp. 4295–4299.

[61] D. Amodei, S. Ananthanarayanan, R. Anubhai, J. Bai, E. Battenberg, C. Case, J. Casper, B. Catanzaro, J. Chen, M. Chrzanowski, A. Coates, G. Diamos, E. Elsen, J. H. Engel, L. Fan, C. Fougnier, A. Y. Hannun, B. Jun, T. Han, P. LeGresley, X. Li, L. Lin, S. Narang, A. Y. Ng, S. Ozair, R. Prenger, S. Qian, J. Raiman, S. Satheesh, D. Seetapun, S. Sengupta, C. Wang, Y. Wang, Z. Wang, B. Xiao, Y. Xie, D. Yogatama, J. Zhan, and Z. Zhu, "Deep speech 2 : End-to-end speech recognition in english and mandarin," in *Proc. ICML*, 2016, pp. 173–182.

[62] R. Schlüter, I. Bezrukov, H. Wagner, and H. Ney, "Gammatone features and feature combination for large vocabulary speech recognition," in *Proc. ICASSP*, 2007, pp. 649–652.

[63] Y. Tian, D. Krishnan, and P. Isola, "Contrastive multiview coding," *arXiv preprint arXiv:1906.05849*, 2019.